Non-hyperbolicity at large scales of a high-dimensional chaotic system

Caroline L. Wormell*

February 3, 2022

Abstract

The dynamics of many important high-dimensional dynamical systems are both chaotic and complex, meaning that strong reducing hypotheses are required to understand the dynamics. The highly influential chaotic hypothesis of Gallavotti and Cohen states that the large-scale dynamics of high-dimensional systems are effectively uniformly hyperbolic, which implies many felicitous statistical properties. We obtain direct and reliable numerical evidence, contrary to the chaotic hypothesis, of the existence of non-hyperbolic large-scale dynamical structures in a mean-field coupled system. To do this we reduce the system to its thermodynamic limit, which we approximate numerically with a Chebyshev basis transfer operator discretisation. This enables us to obtain a high precision estimate of a homoclinic tangency, implying a failure of uniform hyperbolicity. Robust non-hyperbolic behaviour is expected under perturbation. As a result, the chaotic hypothesis should not be *a priori* assumed to hold in all systems, and a better understanding of the domain of its validity is required.

1 Introduction

Most complex systems have chaotic dynamics on a large set of parameters: such systems include those in statistical mechanics, and the Earth's climate system. The chaotic dynamics of such systems being almost universally too complicated to treat from rigorous first principles, general simplifying principles are necessary to understand the system's most important components. When the system is spatially structured, such as in climate models, these components are often the dynamics taking place on large spatial scales [48].

The paradigmatic subclass of chaotic systems are uniformly hyperbolic systems, which have a uniform splitting between expanding and contracting directions [11]. Because of their simple geometry, these systems are very amenable to study. Without good hyperbolicity assumptions, however, our rigorous knowledge of multidimensional chaotic systems is meagre [8]. This is a major problem, because real-life examples of hyperbolic chaotic dynamics are very rare [26], whereas strong violations of hyperbolicity are common [31].

Nonetheless, it is conjectured that, when considered at large scales, typical chaotic dynamics resolve as hyperbolic [17]:

Hypothesis 1 (Gallavotti–Cohen [18, 19]) *The macroscopic dynamics of a (high-dimensional) chaotic system on its attractor can be regarded as a transitive hyperbolic ("Anosov") evolution.*

*Laboratoire de Probabilités, Statistique et Modélisation (LPSM), Sorbonne Université, Université de Paris
email: wormell@lpsm.paris
ORCID: 0000-0003-2953-6493

In fact, many "nice" statistical properties possessed by uniformly hyperbolic systems are also found in the macroscopic-scale dynamics of certain large non-uniformly hyperbolic systems. These properties include existence of physical invariant measures, exponential mixing and large deviation laws [27, 29]. Hypothesised mechanisms include emergent stochastic effects in coupled systems [51, 52], matching of topological equivalency classes between different subsystems under perturbations [52], and generic distribution of singularities in the system [41]. The chaotic hypothesis suggests that general high-dimensional chaotic systems may be studied using techniques developed for uniformly hyperbolic systems, an idea which has been much taken up in the geophysics literature [21, 30].

However, potential counter-examples arise when considering the response of the physical invariant measure to dynamical perturbations. Hyperbolic systems are known to have a so-called "linear response", that is to say their statistics vary differentiably when a parameter of the chaotic system is varied [40]: many smooth non-uniformly hyperbolic systems on the other hand fail to have a linear, or even a continuous response [1, 3]. This can be traced to the failure of the physical invariant measure's derivative to exist in a function space where the transfer operator decays summably under iteration (e.g. has a spectral gap) [1, 20]. While in many geophysical systems linear response theory has been successful [5, 39, 28], certain ones appear to respond non-differentiably to perturbations in broad regimes [15, 13], where linear response would not be excluded through slow mixing of general smooth functions [46]. Nonetheless, although it is commonly accepted that the chaotic hypothesis implies some reasonable expectation of structural stability, it is debatable that linear response falls outside the scope of the chaotic hypothesis, because the hypothesis (1) only pertains to individual systems, whereas a linear response is a property of a family of systems [51], notwithstanding that the existence of a formal linear response candidate is a good indicator of the existence of linear response [1].

In recent times, linear response behaviours of complex chaotic systems have been investigated through the increasingly popular model of mean-field coupled maps. These are systems composed of many chaotic subsystems that interact with each other through a mean-field [23]. They are a subset of globally-coupled maps [12]. As the number of subsystems tends to infinity, the large-scale behaviour of these systems can be described by a so-called thermodynamic limit system [38, 24]. These limit systems may exhibit non-trivial and sometimes complex dynamics [44, 14]. With certain smooth hyperbolic subsystems and sufficiently weak couplings, linear responses have been proven to exist in thermodynamic limit systems [45, 16]. On the other hand, [52] presented a mean-field coupled system whose thermodynamic limit's response to perturbations appeared to be non-smooth. This was argued to be the result of an apparent structural similarity between the thermodynamic limit and the non-uniformly hyperbolic Hénon map, for which linear response fails.

The goal of this paper is to furnish an explicit example of non-hyperbolic structures in a thermodynamic limit system similar to that of [52]. The non-uniformly hyperbolic limit system we present has a homoclinic orbit whose stable and unstable directions are tangent to each other, a non-hyperbolic structure which is definitionally excluded in uniformly hyperbolic dynamics [11]. Because the thermodynamic limit system's attractor contains this homoclinic tangency, it violates Hypothesis 1.

We note that our result does not exclude that, despite the non-hyperbolic structure, the system may still have some kind of non-uniform hyperbolic dynamics on some attractor. However, we only expect hyperbolicity in the dynamics in the sense that Lyapunov exponents exist and are bounded away from zero almost everywhere [54]. This is a notably less powerful property than that of Hypothesis 1, and in particular does not imply most of the favourable statistical properties mentioned above.

Apart from self-evidently demonstrating a failure of uniform hyperbolicity for a single limit system, the existence of a generic homoclinic tangency also suggests so-called wild dynamical phenomena on a generic set of nearby limit systems. Examples include the existence of infinitely many sinks (*i.e.* stable periodic orbits), each with their own basin of attraction [33, 6, 7], or more relevantly, of other tangencies between stable or unstable manifolds, which is to say the persistence of

non-hyperbolic behaviour [37]. Thus, the homoclinic tangency we obtained for one system would imply a violation of the chaotic hypothesis for an $O(1)$-size open set of nearby systems.

Our evidence for the homoclinic tangency is numerical. To approximate the infinite-dimensional limit system, we will apply Chebyshev Galerkin discretisations for the transfer operators that describe the thermodynamic limit [50, 4], using the software package `Poltergeist.jl` [49]. Such discretisations are very accurate and efficient in approximating such objects. To obtain the homoclinic tangency in this system we will use a shooting method. With these methods the homoclinic tangency is estimated to a very high accuracy. This furnishes very strong evidence of its existence.

The paper is structured as follows. In Section 2, the mean-field coupled system and its thermodynamic limit are presented, and in Section 3 the mathematical objects required to describe a homoclinic tangency are introduced. In Sections 4-5 numerical methods are presented: first the scheme to approximate the thermodynamic limit map, and then the method to find the homoclinic tangency. The results are presented in Section 6 and in Section 7 implications and further directions are discussed.

2 Model

2.1 Mean-field system

We introduce a mean-field system, similar to those proposed in [52], whose dynamic variables are $M \gg 1$ one-dimensional chaotic subsystems $q^{(j)}$ coupled together via a mean field Φ. These chaotic subsystems $q^{(j)} \in [-1, 1]$ each evolve according to smooth, individually hyperbolic (in fact uniformly-expanding) chaotic dynamics

$$q_{n+1}^{(j)} = f_{t\Phi_n}(q_n^{(j)}), \tag{1}$$

modulated by a mean field of the $q_n^{(j)}$

$$\Phi_n = \frac{1}{M}\sum_{j=1}^{M} q_n^{(j)} \tag{2}$$

and a fixed parameter $t \geq 0$ which determines the strength of the coupling.

For the subsystem dynamics we choose

$$f_\alpha(q) = \mathfrak{d}(q) + g(\alpha)(1 - \mathfrak{d}(q)^2), \tag{3}$$

where $\mathfrak{d}(q) := 2q - \operatorname{sign} q$ is the doubling map on $[-1, 1]$, and

$$g(\alpha) = \tfrac{3}{16}\cos 8\alpha \in (-\tfrac{3}{16}, \tfrac{3}{16}).$$

These maps, given in Figure 1, are piecewise analytic maps of the interval, with two full branches. They are uniformly expanding, with each $|f'_\alpha| \geq \frac{5}{4} > 1$.

Dynamically, the choice of f (in particular of g) encourages the $q^{(j)}$ to take higher values (increasing Φ_{n+1}) for Φ_n close to zero, and towards $q = -1$ for Φ_n appropriately far from zero. For $t \lesssim 3$, this induces quasi-unimodal dynamics in the mean position of the $q^{(j)}$'s.

2.2 Thermodynamic limit reduction

Because the $q^{(j)}$ are exchangeable, the macroscopic aspects of the system should be expressible as functions of the distribution of the $q^{(j)}$ at fixed times.

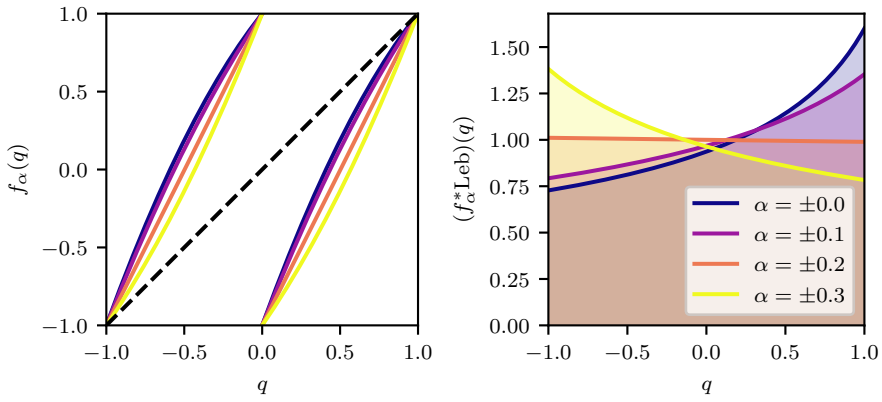

Figure 1: Top: graph of the microscopic maps f_α for some representative values of α.
Bottom: for various α, the action of f_α on Lebesgue measure: that is, $\mathcal{L}_\alpha 1$ for various values of α. Note that because the Lebesgue measure of the domain $[-1, 1]$ is 2, these measures are actually *twice* a probability measure.

It is in fact possible to use this exchangeability to form an exact closure of the system (1-2) in terms of precisely this empirical distribution $\mu_n = \frac{1}{M}\sum_{j=1}^{M} \delta_{q_n^{(j)}}$:

$$\mu_{n+1} = (f_{t\Phi_n})_* \mu_n,$$
$$\Phi_n = \int_{-1}^{1} q \, \mathrm{d}\mu_n(q),$$

where $(f_{t\Phi_n})_*$ is the push-forward of $f_{t\Phi_n}$. Statistics of the $q_n^{(j)}$ can then be recovered through averages over μ_n. As the number of subsystems $M \to \infty$ we can expect the discrete empirical measures μ_n to converge to probability distributions with appropriately smooth Lebesgue densities [24]. In a mild abuse of notation, we will henceforth use μ_n to refer to these density functions. We can thus rewrite our dynamics as

$$\mu_{n+1} = \mathcal{L}_{t\Phi_n} \mu_n, \tag{4}$$
$$\Phi_n = \varphi \mu_n \tag{5}$$

where $\mathcal{L}_\alpha$ is the transfer operator of f_α, with explicit expression

$$(\mathcal{L}_\alpha h)(x) = \sum_{x \in f_\alpha^{-1}(y)} \frac{h(y)}{f_\alpha'(y)}, \tag{6}$$

and the functional φ is given $\varphi\mu := \int q\mu(q)\,\mathrm{d}q$.

While the system (4-5) can be reformulated as a delay equation in mean field Φ_n using the theory of transfer operator cocycles [52], we will solve it as a function of the measure distribution

$$\mu_{n+1} = F_t(\mu_n) := \mathcal{L}_{t\varphi\mu_n} \mu_n. \tag{7}$$

These maps F_t are our thermodynamic limit systems: they sometimes known as self-consistent transfer operators [44, 45].

Because we have assumed that μ_n are smooth, absolutely continuous probability measures, we assume that the dynamics takes place within the space U of positive, twice-differentiable densities that integrate to 1 on $[0, 1]$. However, we can use the uniform analyticity of the maps f_α to further restrict the thermodynamic limit dynamics F_t to act on a scale of function spaces on which it has relatively nice compactness properties.

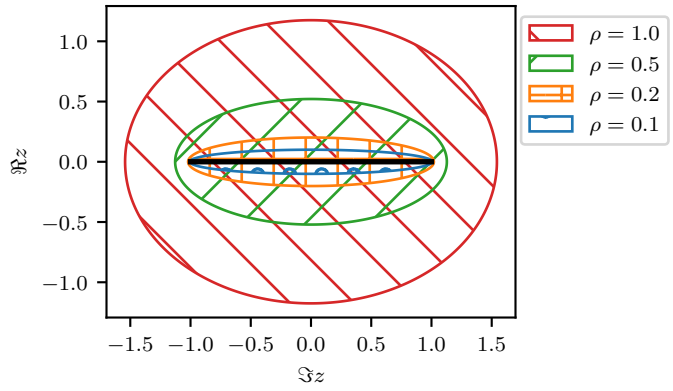

Figure 2: Bernstein ellipses for various parameters ρ.

2.3 Hardy function spaces

The Banach spaces we use are Hardy spaces H_ρ, $\rho > 0$ of analytic functions. For small enough ρ, the sets $H_\rho \cap U$ are invariant sets of the F-dynamics on U. In fact, for any sufficiently large $C > 0, N \in \mathbb{N}$, the sets $\{h : \|h\|_{H_\rho} \leq C\} \cap U$ are attracting invariant sets[1] for some iterate F^N.

The domain of a function in H_ρ is the Bernstein ellipse E_ρ:

$$[-1, 1] \subseteq E_\rho = \cos\left([0, \pi] + i[-\rho, \rho]\right) \subset \mathbb{C}.$$

These are ellipses in the complex plane centred at 0 with semi-axes $\cosh\rho > 1$ and $\sinh\rho > 0$: a range are plotted in Figure 2. The Hardy space H_ρ is composed of continuous complex functions on E_ρ which are analytic on its interior, equipped with the supremum norm

$$\|h\|_\rho = \sup_{z \in E_\rho} |h(z)|.$$

As an edge case, the space H_0 is simply the space of continuous functions $C^0([-1, 1], \mathbb{C})$.

Now, because of its definition through function composition (6), the transfer operator $\mathcal{L}_\alpha$ is bounded from smaller-ρ Hardy spaces into larger-ρ ones [4].

In particular, if $0 < R \leq R_{\max} := 0.5$ and $r \geq 0.93R$, one can show that all $\alpha \in \mathbb{R}$ that $f_\alpha^{-1}(E_R)$ is a subset of E_r. Hence, if $h \in H_r$,

$$\begin{aligned}
\|\mathcal{L}_\alpha h\|_R &= \sup_{z \in E_R} \left| \sum_{w \in f_\alpha^{-1}(z)} \frac{h(w)}{f'_\alpha(w)} \right| \\
&\leq 2 \sup_{w \in f_\alpha^{-1}(E_R)} \left| \frac{h(w)}{f'_\alpha(w)} \right| \\
&\leq \frac{2 \sup_{w \in E_r} |h(w)|}{\inf_{w \in f_{\alpha^{-1}(E_R)}} |f'_\alpha(w)|} \\
&\leq 1.85 \|h\|_r, \qquad (8)
\end{aligned}$$

[1] We have that $\mu_n = F_t^n(\mu_0) = \mathcal{L}_{\alpha_{n-1}} \cdots \mathcal{L}_{\alpha_0} \mu_n$ for some α_k depending on μ_0. Because $\{\mathcal{L}_{\alpha_k}\}$ forms a cocycle of transfer operators uniformly bounded in both H_ρ and C^2, there exists some N such that each $\mathcal{L}_{\alpha_{N+n}} \cdots \mathcal{L}_{\alpha_n}$ is a contraction on both $H_\rho \cap U$ and $C^2 \cap U$ in their respective norms. In particular, μ_n will converge exponentially in C^2 to the time-dependent absolutely continuous invariant measure of the cocycle, which lies in H_ρ and has uniformly bounded H_ρ norm.

In particular, every $\mathcal{L}_\alpha$ is uniformly bounded as an operator $H_r \to H_R$ for $R \in (0, R_{\max}]$ and $r \geq 0.93R_{\max}$.

This means $\mathcal{L}_\alpha$ is bounded as an endomorphism on both H_r and H_R since $\|\cdot\|_r \leq \|\cdot\|_R$ for $r \leq R$. Better than this, inclusions between Hardy spaces of different parameters are very strongly compact, in fact nuclear. This is a simple fact falling out of Fourier analysis [47]. Hence as an endomorphism on H_r, the transfer operator $\mathcal{L}_\alpha$ has the same strong compactness properties uniformly in α.

On these Hardy spaces, the transfer operator also has a very nice perturbation theory. It is a standard fact of complex analysis the differentiation operator ∂_q and its iterates ∂_q^k are also bounded as operators $H_R \to H_r$ for any $r < R$. A particular consequence of this is that, since the derivatives of the transfer operator with respect to dynamical perturbations, that is $\frac{\mathrm{d}^k \mathcal{L}_\alpha}{\mathrm{d}\alpha^k}$, can be expressed as linear combinations of $\partial_q^j \mathcal{L}_\alpha, j \leq k$ [43, Section 2.3], these derivatives are also bounded as operators $H_r \to H_r$. In our setting, the map $\alpha \mapsto \mathcal{L}_\alpha$ is therefore a C^∞ function $\mathbb{R} \to L(H_r, H_r)$ for appropriate positive choices of $r < 0.93R_{\max}$. This justifies the perturbation theory used in the rest of the paper.

3 Manifolds and tangencies

It is now necessary to define the manifold structure of F_t, which will allow us to speak to its hyperbolicity or absence thereof.

Let us suppose that we have a differentiable dynamical system F acting on an affine subspace M of a Banach space with tangent space TM which we may naturally identify with $M \times (M - m^*)$ for any $m^* \in M$. The stable manifold of a point $x \in M$ is the set of points near x whose forward orbits converge to that of x:

$$\mathcal{V}_x^s = \{y \in M : \lim_{n\to\infty} d_M(F^n x, F^n y) = 0\},$$

where d_M is the metric on M. The local stable manifold of x is the set of such points which additionally do not leave some small δ-neighbourhood of x:

$$\mathcal{V}_x^{s,\mathrm{loc}} = \{y \in M : \lim_{n\to\infty} d_M(F^n x, F^n y) = 0, \sup_{n\in\mathbb{N}} d_M(F^n x, F^n y) \leq \delta\} \subset \mathcal{V}_x^s.$$

Similarly, when F is a diffeomorphism, the unstable manifold of x is the set of points with *backward* orbits converging to that of x:

$$\mathcal{V}_x^u = \{y \in M : \lim_{n\to\infty} d_M(F^{-n} x, F^{-n} y) = 0\}.$$

Along hyperbolic trajectories of x and under reasonable conditions, these stable and unstable manifolds are indeed manifolds. Furthermore, if the range of $D_x F$ is dense in $T_x M$ for all x, then the global stable manifold $\mathcal{V}_x^s$ has the same codimension as the local stable manifold [22] (we prove this for our maps F_t in the Appendix). On the other hand, if the kernel of $D_x F$ avoids the unstable space then the global unstable manifold V_x^u can be expected to have the same dimension as the local unstable manifold.

We can extend these notions of stable and unstable manifolds onto the tangent bundles. For $x \in M$ let $D_x F : TM \to TM$ be the differential of F, that is to say that for all tangent vectors $v \in TM$

$$F(x + \epsilon v) = F(x) + \epsilon D_x F v + \mathcal{O}(\epsilon^2).$$

The *stable subspace* (resp. *unstable subspace*) at x, E_x^s (resp. $E^u(x)$) $\subseteq TM$, is then the set of tangent vectors at x which converge to zero under the action of DF (resp. F^{-1}):

$$E_x^s = \{v \in T_x M : \lim_{n\to\infty} D_x F^n \, v = 0\}$$
$$E_x^u = \{v \in T_x M : \lim_{n\to\infty} D_x F^{-n} \, v = 0\},$$

where D_xF is the Jacobian (or differential) of F. These are respectively tangent to local stable and unstable manifolds [11].

Because our limiting dynamics F_t given in (7) are not diffeomorphisms,[2] the unstable manifolds and subspaces are ill-defined. However, it is possible to define the unstable manifold (resp. subspace) of a backward orbit $(x_{-n})_{n\in\mathbb{N}}$: this can be achieved using the machinery of natural extensions. If x_* is a fixed point then for convenience we will define $\mathcal{V}^u_{x_*}$ (resp. $E^u_{x_*}$) to be the unstable manifold (resp. subspace) of the orbit $x_{-n} \equiv x_*$.

If x is a fixed point, then $\mathcal{V}^s_x$ are the set of points with orbits converging to x, and $\mathcal{V}^u_x$ are the set of points with orbits emanating from x; furthermore, provided that the differential D_xF is hyperbolic (*i.e.* its spectrum is bounded away from the unit circle), E^s_x is the span of the stable eigenspaces and E^u_x the span of the unstable eigenspaces.

A separation between unstable and stable subspaces is a key property of most well-behaved chaotic systems. A system is *uniformly hyperbolic* if at every point $x \in M$ the tangent space has an F-invariant splitting $T_xM = E^s_x \oplus E^u_x$, and there are constants $c > 0$, $\gamma < 1$ such that for all $x \in M$,

$$\|D_xF^n{}_{|E^s_x}\| \le c\gamma^n,$$
$$\|D_xF^{-n}{}_{|E^u_x}\| \le c\gamma^n.$$

According to Hypothesis 1, the F_t are supposedly transitive and (uniformly) hyperbolic on their respective attractors. These two conditions together are the Axiom A of Smale [11].

One generic mechanism to generate non-uniformly hyperbolic dynamics is via homoclinic tangencies. A *homoclinic tangency* in a map $F : M \circlearrowleft$ is a hyperbolic fixed point p of F together with a different point $q \in \mathcal{V}^u_p \cap \mathcal{V}^s_p$ such that $\mathcal{V}^u_p$ and $\mathcal{V}^s_p$ are tangent at q [42]. In particular, because $E^{s/u}_q = T_qV^{s/u}_p$, the stable and unstable subspaces E^s_q and E^u_q have non-trivial intersection, implying non-hyperbolicity of the given map F.

It is easy enough to show that a homoclinic tangency is equivalent to having that $q \in \mathcal{V}^u_p$ with $\lim_{n\to\infty} F^n(q) = p$ and $\lim_{n\to\infty} \|D_qF^n|_{E^u_q}\| \to 0$, because the stable subspaces $E^s_\cdot$ vary continuously at p since it is a hyperbolic fixed point.

4 Spectral methods

In Section 2.3 we discussed the strong compactness and regularity properties of F_t in certain Hardy spaces. This allows us to very effectively approximate the dynamics of the F_t and invariant manifolds on the computer, through projection onto a basis of Chebyshev polynomials.

The Chebyshev polynomials $T_k, k = 0, 1, \ldots$ are a polynomial family orthogonal in $L^2_{\text{Cheb}} := L^2([-1, 1], \mathrm{d}x/\sqrt{1-x^2})$:

$$\int_{-1}^{1} T_k(x)T_j(x)\frac{\mathrm{d}x}{\sqrt{1-x^2}} = w_k\delta_{jk},$$

where $w_k := \frac{\pi(1+\delta_{0k})}{2}$. They have explicit expression

$$T_k(x) = \cos(k\cos^{-1}x),$$

from which falls out a natural connection to Fourier series under the one-to-two transformation $x = \cos\theta$.

Chebyshev approximation is well-adapted to this compact inclusion. Let P_n be the L^2_{Cheb} orthogonal projection onto the first n Chebyshev polynomials. It is a standard result that if

[2]Note that, at the expense of complicating the perturbation theory, we could make the maps F_t closer to diffeomorphisms by adding hidden dynamics $r_{n+1} = \frac{1}{2}(r_n + \mathbf{1}_{q_n>1/2}) \in [0, 1]$ and choosing F_t to act on an appropriate subset of a Triebel space [2].

$C_{R-r} := (1 - e^{-(R-r)})^{-1}$ then for $0 \leq r < R$ we have [47]

$$\|(I - P_n)h\|_r \leq C_{R-r} e^{-(R-r)n} \|h\|_R. \tag{9}$$

On the other hand, from (8) we know that for $r \leq 0.93R$, $R \in (0, R_{\max}]$

$$\sup_{\alpha \in \mathbb{R}} \|\mathcal{L}_\alpha h\|_r \leq 0.85 \|h\|_R.$$

From these two equations we therefore know that for such r, R and for all $\alpha \in \mathbb{R}$,

$$\|(I - P_n)\mathcal{L}_\alpha\|_r \leq \|I - P_n\|_{r \to R} \|\mathcal{L}_\alpha\|_{R \to r} \leq 0.85 C_{R-r} e^{-(R-r)n}.$$

This implies that the so-called Chebyshev Galerkin approximation $P_n \mathcal{L}_\alpha$ of the transfer operator $\mathcal{L}_\alpha$ converges exponentially to the true operator, and thus so do its spectrum and eigenvalues [4]. This can also be extended to more complex functions of $\mathcal{L}_\alpha$ such as the differential of F_t defined in (10) below.

The Galerkin approximations $P_n \mathcal{L}_\alpha$ are finite-dimensional, and such operators can be easily computed to high accuracy and faithfully represented using the theory of Chebyshev series [47]. In particular, if we represent the image of the projection P_n in the Chebyshev basis $\{T_k\}_{k=0,\ldots,n-1}$, then the finite-rank operators $P_n \mathcal{L}_\alpha|_{P_n}$ can be represented as $n \times n$ matrices in this basis, with entries

$$L_\alpha^{jk} = w_k^{-1} \int_{-1}^{1} (\mathcal{L} - \alpha T_k)(x) T_j(x) \frac{\mathrm{d}x}{\sqrt{1 - x^2}}.$$

These entries can be computed very efficiently by interpolating the action of the operator on a sufficiently large number of Chebyshev nodes, which are cosines of evenly-spaced Fourier nodes. Indeed, we have exponential convergence in the number of interpolating points N [47]

$$L_\alpha^{jk} = w_k^{-1} N^{-1} \sum_{l=0}^{N-1} (T_j \, \mathcal{L} T_k) \left(\cos \frac{(2l+1)\pi}{2N} \right) + \mathcal{O}(e^{-R_{\max} N}).$$

These sums themselves may be computed for all $j < N$ very quickly using the fast Fourier transform. Further details may be found in [50].

In practice, we note that when simulating the F dynamics acting on a specific function h, it is often more efficient to approximate the action of F directly

$$F(h) \approx P_n(\mathcal{L}_\alpha h)$$

rather than constructing a numerical representation of the operator $P_n \mathcal{L}_\alpha$ and applying it to h. This is because at every step α and therefore $\mathcal{L}_\alpha$ is different, and there is therefore no time saved by storing a representation of the transfer operator.

5 Numerically obtaining the homoclinic

Given that we can compute that action and derivatives of the thermodynamic limit map F_t to high accuracy, it then remains to present a method to compute other dynamical objects associated with the thermodynamic limit. In this section, these objects and the methods to compute them are described, starting from the unstable fixed point (Section 5.1), through its local manifold approximations (Section 5.2) to the homoclinic tangency itself (Section 5.2).

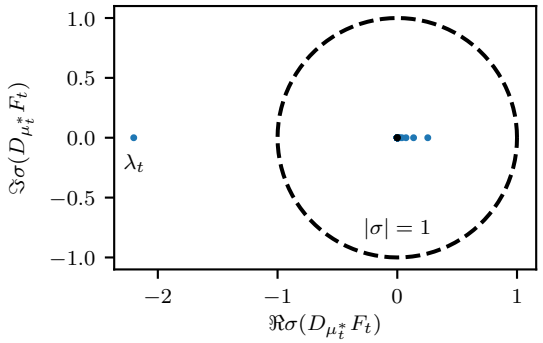

Figure 3: In blue, the (ρ-independent) H_ρ spectrum of the differential $D_{\mu_t^*}F_t$ of the fixed point of F_t, computed for $t = 2.8$ using `Poltergeist.jl`. This package uses an adaptive-order Galerkin truncation [50] and computes eigenvalues via the QR algorithm [35]. Away from zero, the spectrum is uniformly stable to perturbations in t.

5.1 Hyperbolic fixed point

For all $t > 0$ the thermodynamic limit system F_t given in (7) has a unique fixed point μ_t^* with $\Phi_t^* := \varphi\mu_t^*$ lying between $(0, \pi/16t)$. If we define $\mu_{\text{acim}}(\alpha)$ to be the invariant probability density of transfer operator $\mathcal{L}_\alpha$, then this can be computed numerically[3] simply as $\mu_t^* = \mu_{\text{acim}}(t\Phi_t^*)$ where Φ_t^* solves

$$\Phi_t^* = \varphi\mu_{\text{acim}}(t\Phi_t^*).$$

This equation also gives the existence and uniqueness of the fixed point, as $\alpha \mapsto \varphi\mu_{\text{acim}}(\alpha)$ is strictly decreasing on $[0, \pi/16]$ with a zero at $\alpha = \pi/16$.

At μ_t^* the Jacobian of F_t is given by

$$D_{\mu_t^*}F_t\psi = \mathcal{L}_{t\Phi_t^*}\psi - t\varphi\psi\mathcal{L}_{t\Phi_t^*}\partial_q X_{t\Phi_t^*}, \tag{10}$$

where X_α is given by

$$f_{\alpha+\epsilon}(q) = f_\alpha(q) + \epsilon X_\alpha(f_\alpha(q)) + \mathcal{O}(\epsilon^2) \tag{11}$$

and is explicitly written in the Appendix.

Because our F_t dynamics are restricted to probability densities, we restrict the operator DF_t to functions of zero mean in H_ρ. Under this restriction, $D_{\mu_t^*}F_t$ is hyperbolic in the sense of that its spectrum (which is independent of ρ) uniformly bounded away from the unit circle. In particular, its spectrum outside the unit disc consists of a single eigenvalue $\lambda_t < -1$ (see Figure 3). This unstable eigenvalue has right eigenfunction $e_t^u \in H_\rho$ and left eigenfunctional $d_t^u \in H_\rho^*$. We normalise e_t^u so that $\|e_t^u\|_{L^2_{\text{Cheb}}} = 1$ with $\langle 1, e_t^u\rangle_{\text{Cheb}} > 0$, and we normalise d_t^u to have $d_t^u e_t^u = 1$. We estimate these quantities to near-floating point precision very easily using the Chebyshev spectral methods in Section 4. In the case of e_t^u this may be done adaptively using `Poltergeist.jl`.

[3]This may be computed via bisection on $\Phi_t^* \in [0, \pi/16t]$. For t close to the homoclinic tangency, a faster-converging method however is to compute μ_t^* iteratively as a stable fixed point of the relation $\mu_{m+1} = \frac{2}{3}F_t(\mu_m) + \frac{1}{3}F_t^2(\mu_m)$. Given a sufficiently accurate initial guess, the convergence is justified by considering the Jacobian of this iteration about μ_t^*, which is $D_{\mu_t^*}F_t(\frac{2}{3} + \frac{1}{3}D_{\mu_t^*}F_t)$. This operator has spectral radius bounded by 0.2 for $t \approx t_{\text{ht}}$, which is a result of its spectrum being that of $D_{\mu_t^*}F_t$ under the mapping $z \mapsto \frac{z+2}{3}z$, which almost annihilates the unstable eigenvalue (see Figure 3).

5.2 Local manifold approximations

The fixed point's unstable manifold $\mathcal{V}^u_{\mu^*_t}$, which we write for short as $\mathcal{V}^{u,*}_t$, is parametrised near μ^*_t by

$$\mathcal{V}^{u,*}_t(a) = \mu^*_t + e^u_t a + \tfrac{1}{2} h^u_t a^2 + \mathcal{O}(a^3). \tag{12}$$

where the second-order correction is

$$h^u_t = ((\lambda_t)^2 - D_{\mu^*_t} F_t)^{-1} H_{\mu^*_t} F_t(e^u_t, e^u_t).$$

The tensor $H_{\mu^*_t} F_t$ is the Hessian of F_t at μ^*_t, with an explicit formula given in Appendix 7. Like e^u_t, the function h^u_t is also easy to accurately approximate with spectral methods.

The parametrisation (12) can be chosen to have the useful property that $F_t(\mathcal{V}^{u,*}_t(a)) = F_t(\mathcal{V}^{u,*}_t(\lambda_t a))$. Furthermore, the tangent vectors to $\mathcal{V}^{u,*}_t(a)$ are generated by

$$(\mathcal{V}^{u,*}_t)'(a) = e^u_t + h^u_t a + \mathcal{O}(a^2). \tag{13}$$

At each point $\mathcal{V}^{u,*}_t(a)$ in the unstable manifold, this tangent vector generates its unstable subspace $E^u_{\mathcal{V}^{u,*}_t(a)}$.

It is not *a priori* guaranteed that the global unstable manifold has the same dimension as it does near the fixed point[4], but we can produce a dimension-one global manifold from the local manifold by iteration, provided that its tangent vectors avoid the kernel of DF_t. In our system, the unstable manifold in fact appears to uniformly avoid the kernel: random sampling of both the unstable manifold and the attractor indicates that there is a bound on the contraction rate

$$\sup_{\mu \in \mathcal{V}^{u,*}_t} \|(DF_t|_{E^u_x})^{-1}\| \leq 0.18^{-1}$$

for all $t \in [2.7, 2.83]$. Numerical investigation suggests the existence of an invariant cone on TM which would yield a robust rigorous bound of this sort on the contraction rate.

On the other hand, the fixed point's local stable manifold $p \in \mathcal{V}^{s,\mathrm{loc}}_{\mu^*_t}$, which we write for short as $\mathcal{V}^{s,*}_t$, is close to the kernel of the functional d^u_t, so that for $\mu \in \mathcal{V}^{s,*}_t$,

$$d^u_t(\mu - \mu^*_t) = \mathcal{O}(\|\mu - \mu^*_t\|^2_\rho), \tag{14}$$

for $\mu \in \mathcal{V}^{s,*}_t$. We expect that, for all local stable points $\mu \in \mathcal{V}^{s,*}_t$ and stable tangent vectors $v \in T_\mu \mathcal{V}^{s,*}_t$, the tangent hyperplanes to such an $\mathcal{V}^{s,*}_t$ satisfy

$$d^u_t v = \mathcal{O}(\|\mu - \mu^*_t\|_\rho)\|v\|_\rho. \tag{15}$$

They constitute the stable subspace $E^s_{t,\mu}$ for $\mu \in \mathcal{V}^{s,*}_t$. In the Appendix, we show that $D_\mu F_t$ always has dense range on H_R, implying that the global stable manifold $\mathcal{V}^s_{\mu^*_t}$ also has codimension one.

All these quantities can also be accurately estimated via spectral methods. They converge exponentially to the true estimates in the Hardy space H_R for certain $R > 0$, except notably for the leading left eigenfunctional d^u_t of $D_{\mu^*_t} F_t$ at the fixed point, which will converge exponentially in the dual space H^*_r for small $r \in (0, R)$.

We used the Julia package `Poltergeist.jl` to make and adaptively choose the order of the estimates [50]. The exception again is the left eigenfunctional d^u_t, which we computed iteratively via applying $\mathcal{L}^*$ to a vector of Chebyshev coefficients until convergence was attained. The order of this approximation (*i.e.* the number of Chebyshev coefficients used) was chosen to be approximately that used by `Poltergeist.jl` for estimating the right eigenfunctions[5].

[4] Although it is generic: the kernel of the differential is smaller than that of the transfer operator (see Appendix), which has infinite codimension.

[5] At higher numerical precisions it was also most efficient here to compute eigendata iteratively via the power method, using `Poltergeist.jl` to compute the action of $D_{\mu^*_t} F_t$ on an eigenvector estimate, renormalising and so on.

5.3 Shooting method

Our aim is to find a parameter t and a point $q \in \mathcal{V}_t^{u,*}$ such that $q \in \mathcal{V}_t^{s,*}$ also, with unstable subspace $E_{t,q}^u$ a subset of the stable subspace $E_{t,q}^s$. Because we have good knowledge of the local stable and unstable manifolds near fixed points μ_t^*, we rephrase this as attempting to find a pair (t, a) such that

$$F_t^n(\mathcal{V}_t^{u,*}(a)) \to \mu_t^*, \tag{H1}$$
$$(D_{\mathcal{V}_t^{u,*}(a)} F_t^n)(\mathcal{V}_t^{u,*})'(a) \to 0. \tag{T1}$$

Since $F_t^n(\mathcal{V}_t^{u,*}(a))$ converges towards μ_t^*, we can use the local linearisation of the stable manifold (14) and (H1–T1) becomes equivalent to solving for (t, a)

$$d_t^u(F_t^n(\mathcal{V}_t^{u,*}(a)) - \mu_t^*) \to 0, \tag{H2}$$
$$d_t^u(D_{\mathcal{V}_t^{u,*}(a)} F_t^n)(\mathcal{V}_t^{u,*})'(a) \to 0, \tag{T2}$$

where now the left-hand quantities are one-dimensional instead of lying in a Banach space H_r as before.

One way to satisfy these conditions is to find for each t an $a(t)$ satisfying (T2), and then finding a $(t, a(t))$ satisfying (H2). This turns out to be the most numerically stable option, because when done in this order the roots of both problems are simple and isolated, which is not the case for other approaches[6]. In both cases, because of the finite relative precision ε of floating-point arithmetic, and because μ_t^* is a saddle, we will not in practice be able to compute an orbit converging to μ_t^* by simple shooting. Instead, we must assume that the convergence holds along the orbit up until some $n = n_*$ determined by the floating-point precision, and do some careful error analysis based on the blowup of this error in ϵ.

We eventually chose our floating-point precision to be 159 bits (*i.e.* three times as many bits as the standard double precision), using the GNU MPFR library implemented as the `BigFloat` type in Julia: in particular, the relative precision of the floating-point encoding is $\epsilon \approx 2.7 \times 10^{-48}$. Having progressively refined our guess at lower precisions, as bracketing intervals we chose

$$a \in 0.792\,760\,229\,502\,464\,90 + [0, 2 \times 10^{-17}]$$
$$t \in 2.786\,033\,304\,650\,978\,791 + [0, 2 \times 10^{-18}].$$

To compute $q_t = \mathcal{V}_t^{u,*}(a)$ accurately we apply the approximation (12) to $F^{-n_\epsilon}(q_t) = \mathcal{V}_t^{u,*}(\lambda^{-n_0} a)$, where we choose $n_0 = \lceil \log_{2.19}(\epsilon^{-1/3}) \rceil = 16$. Because $\lambda_t \approx -2.19$ for $t \approx 30$, this gives us an error $|F^{-n}(q_t) - \mu_t^*| = \mathcal{O}(\epsilon^{2/3})$. Because we are shrinking our starting point by $\mathcal{O}(\epsilon^{1/3})$, it also gives us an effective numerical precision of $\mathcal{O}(\epsilon^{2/3})$ rather than the full $\mathcal{O}(\epsilon)$.

To estimate the tangent vector at q, $(\mathcal{V}_t^{u,*})'(a)$, we estimate

$$(\mathcal{V}_t^{u,*})'(a) = \lambda_t^{-2n_0} \left(D_{\mathcal{V}_t^{u,*}(\lambda_t^{-n_0} a)} F_t^{n_0}\right) \left(D_{\mathcal{V}_t^{u,*}(\lambda_t^{-2n_0} a)} F_t^{n_0}\right) (\mathcal{V}_t^{u,*})'(\lambda_t^{-2n_0} a)$$

where $\mathcal{V}_t^{u,*}$ and its derivative are computed using (13) when they are evaluated at $\lambda_t^{-2n_0} a$. This also returns an error of $\mathcal{O}(\epsilon^{2/3})$.

For fixed $n = n_1$, the left-hand sides of (H2) and (T2) are monotone in a and t over sufficiently small intervals. We therefore fixed n in these two equations and used interval subdivision over parameters of t to find $(t, a(t))$ satisfying (H2), where for each t we found (again by subdivision) $a(t)$ satisfying (T2).

We fixed $n_1 = 5 + \lceil \log_{2.19 \times 0.255^{-2}} \epsilon^{-2/3} \rceil = 12$, which is approximately when we expect the quantities in (H2) and (T2) to reach their minimum within the bounds of our numerical precision.

[6] To lowest order, the left-hand side of (H2) is $\sim (a - a_{\mathrm{ht}})^2 + (t - t_{\mathrm{ht}})$ and the left-hand side of (T2) is $\sim (a - a_{\mathrm{ht}}) + (t - t_{\mathrm{ht}})$.

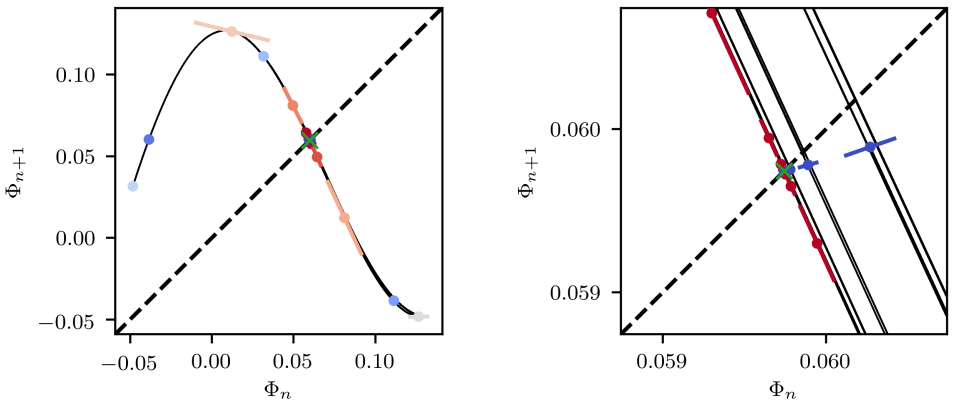

Figure 4: Left: plot of the homoclinic orbit (dots) and its covariant unstable vectors (lines centred on dots), plotted in colours from red (n small) to blue (n large), projected onto delay coordinates in the mean-field Φ_n. The attractor of the F dynamics is plotted in black, and the fixed point $\mu^*_{t_{\mathrm{ht}}}$ is plotted as a green cross. Note that the unstable vectors are as expected all tangent to the attractor. Right: detail near the fixed point. The homoclinic orbit emanates from (red) and falls into (blue) the fixed point, with the unstable vector clearly expanded (resp. contracted) by the dynamics.

This choice can be explained as follows. The homoclinic orbit $F^n(\mathcal{V}^{u,*}_t(a))$ approaches μ^*_t as $\mathcal{O}(\tilde{\lambda}^n_t)$, where $\tilde{\lambda}_t \approx 0.255$ is the spectral radius of the fixed point differential $D_{\mu^*_t}F$ in the stable subspace. Because d^u_t captures the local stable manifold of μ^*_t to first order, it has a second-order error in the distance to the fixed point, and so the quantities in (H2) and (T2) decay as $\mathcal{O}(0.255^{2n})$. On the other hand, the initial error grows as $\mathcal{O}(\epsilon^{2/3}\lambda^n_t)$. This halts the decay of the quantities we are interested in at $n \approx n_1$, and the magnitudes of these quantities bottom out at $\epsilon^{2/3(1+\log 0.255^{-1}/2\log 2.19)} = 3 \times 10^{-20}$.

Our shooting method (as well as routines to compute stable and unstable manifolds in extended floating point) is contained in the supplementary file `quadratic3.jl`.

6 Results

We can now present the results we used to compute these quantities.

6.1 Existence of a homoclinic tangency

Using the shooting method we obtained the following (non-rigorously validated) estimates for the parameters of a homoclinic tangency:

$$t_{\mathrm{ht}} = 2.786\,033\,304\,650\,978\,792\,184\,539\,709\,484\,2 \pm 2 \times 10^{-31}$$
$$a_{\mathrm{ht}} = 0.792\,760\,229\,502\,464\,909\,617\,483\,088\,582\,5 \pm 2 \times 10^{-31}.$$

The relevant homoclinic orbit is plotted with its unstable vectors in Figure 4, and the quantities (H2–T2) we aimed to minimise are plotted in Figure 5. In Figure 5 we also verify that the original homoclinic tangency conditions (H1–T1) are also satisfied.

The precision achieved in these estimates is of a comparable $\epsilon^{2/3} = 2 \times 10^{-32}$ error with our 159-bit floating point precision. The quantities in (H2) and (T2) reach their minima a little before

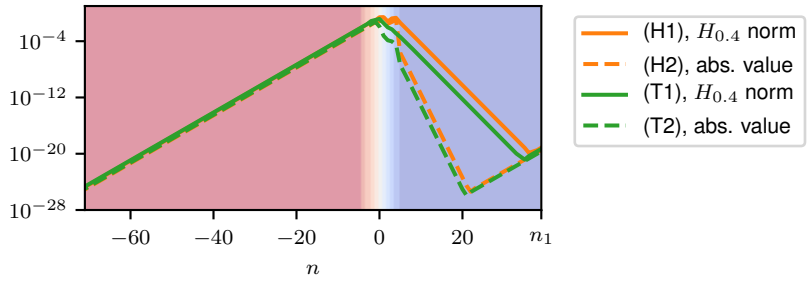

Figure 5: The norm of the left-hand side of various equations (which theoretically should converge to zero as $n \to \infty$) for our numerical approximation of the homoclinic tangency. Background colours correspond to those in Figure 4.

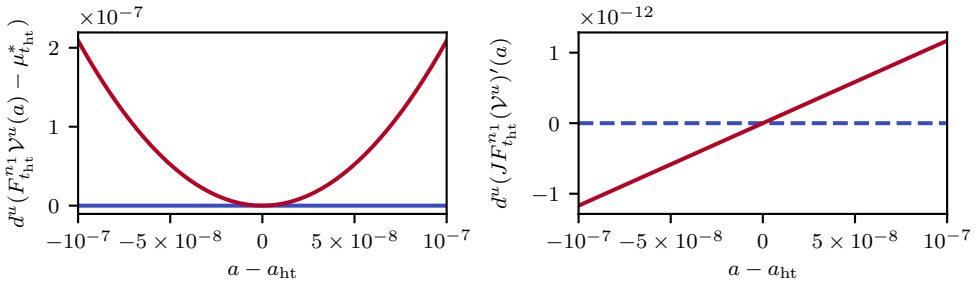

Figure 6: Left: the unstable manifold near the homoclinic point $F^{n_1}(\mathcal{V}^u_{t_{\rm ht}}(a_{\rm ht}))$ (red) and the linearised stable manifold (blue). These are projected to one dimension with the eigenfunctional $d^u_{t_{\rm ht}}$. Right: the same projection of the unstable manifold's derivative $\frac{d}{da}F^{n_1}(\mathcal{V}^u_{t_{\rm ht}}(a_{\rm ht}))$ (red) and of the linearised stable manifold (blue).

$n = n_1 = 12$, as predicted, and these minima are of the order of $\epsilon^{2/3(1+\log 0.255^{-1}/2\log 2.19)} = 8\times10^{-21}$, also as predicted.

These results are obtained to a high precision, with all apparent errors being of the predicted order. Because the thermodynamic limit system F_t has very high regularity with strong compactness properties, it is therefore essentially guaranteed that such a homoclinic tangency exists.

We also have evidence that the homoclinic tangency is generic in two ways that together suggest persistent wild, non-hyperbolic behaviour under perturbation [6].

Firstly, the homoclinic tangency is quadratic, that is to say that the tangency between the stable and unstable manifolds is a quadratic tangency. The functional d^u_t measures the distance to the local stable manifold of μ^*_t (to first order in the distance from μ^*_t): in Figure 6 we plot the distances to the unstable manifold at $F^n_{t_{\rm ht}}(\mathcal{V}^u_{t_{\rm ht}}(a))$ for $a \approx a_{\rm ht}$, as well as the derivative of this with respect to a. The derivative is smooth and clearly has non-zero slope at $a = a_{\rm ht}$, meaning the tangency is quadratic. This could be explicitly demonstrated in future work by showing $\frac{\mathrm{d}^2}{\mathrm{d}a^2}F^{n_1}_{t_{\rm ht}}(\mathcal{V}^u_{t_{\rm ht}}(a)) \neq 0$.

Secondly, we also have strong evidence that tangency is perturbed generically, in the sense that for all t slightly less than $t_{\rm ht}$ the unstable manifold around the homoclinic orbit is locally separated from the stable manifold (see Figure 7). In fact, as we might expect, the displacement of the unstable manifold as t is varied is linear and transversal to the stable manifold. If our system was a diffeomorphism, satisfaction of these criteria for a quadratic tangency would imply the existence

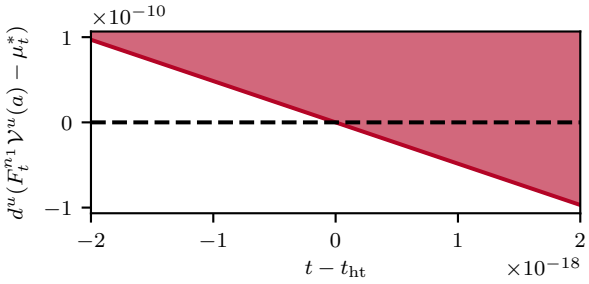

Figure 7: In block colour, the displacement from the local unstable manifold to the local stable manifold at $F^{n_1}(\mathcal{V}_t^u(a))$ for $a \approx a_{\mathrm{ht}}$ and $t \lesssim t_{\mathrm{ht}}$, projected onto one dimension using d_t^u. As a line, the minimum value attained for given t.

of heteroclinic tangencies (*i.e.* non-uniform hyperbolicity) on an open set of parameters t [34, 37].

To this end, we find that at $t = t_{\mathrm{ht}}$, the fixed point is *sectionally dissipative*: the differential of the fixed point has leading eigenvalue $\lambda_t < -1.9898$ and all other eigenvalues having modulus less than $0.255 < |-1.9818|^{-1}$, meaning that any product of two eigenvalues has modulus less than one. As a result, we can also expect a Baire generic Cantor set of parameters t where an infinite number of stable periodic orbits coexist [37, 7]

6.2 Dynamics at $t = t_{\mathrm{ht}}$

Although we have that the map F_t is non-uniformly hyperbolic, Hypothesis 1 applies only to dynamics on the attractor of the system, which is to say, presumably, on the attractor of the macroscopic dynamics. We therefore wish to have some idea of the macroscopic dynamics's attractor, and in particular whether homoclinic tangency lies on it.

We simulated the thermodynamic limit dynamics at $t = t_{\mathrm{ht}}$ using `Poltergeist.jl` [52, Appendix B]. The dynamics is chaotic: through simulations on 10 time series of 10^4 realisations we estimated the leading Lyapunov exponents as $\lambda_1 = 0.381 \pm 0.005 > 0$, $\lambda_2 = -1.150 \pm 0.003 < 0$, $\lambda_3 = -2.015 \pm 0.004 < 0$. The existence of a positive Lyapunov exponent suggests the attractor has dimension at least 1: the estimates on the Lyapunov exponents then suggest that its Kaplan-Yorke dimension is 1.249 ± 0.002. The dynamics also appears to be exponentially mixing over a timescale $t_{1/e} \approx 9$. Because there appear to be Lyapunov exponents that are well-defined and away from zero, it is reasonable to claim that the dynamics on the attractor are indeed non-uniformly hyperbolic, if only in a rather weak sense [54].

Under this assumption that the attractor is chaotic, there is substantial evidence that the fixed point's unstable manifold, and hence the homoclinic orbit actually lies on this attractor. In Figure 4 it is clear that the attractor contains long unstable manifolds that pass near the fixed point in a direction generally parallel to the unstable vector of the fixed point. We therefore expect that these unstable manifold must have intersections with the stable manifold of the fixed point, implying that the fixed point lies on the attractor. To support this, we took a long time series of F_t dynamics and collected the $H_{0.4}$ distance of points in the time series to the fixed point μ_t^* (see Figure 8). There is a regular scaling of the physical measure of the F_t dynamics as the distance from the fixed point tends to zero corresponding with a measure dimension at the fixed point of around 1.6. The closest point in the time series was 6×10^{-7} away from the fixed point in $H_{0.4}$ distance, which is of the order expected when the true minimum distance to the attractor is zero.

Because the attractor contains the fixed point and the system is chaotic (so cannot be confined to the stable manifold of the fixed point), the attractor must also contain the unstable manifold of

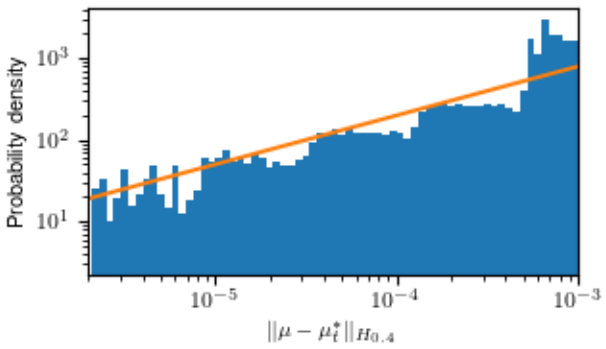

Figure 8: In blue, a histogram of the Hardy space $H_{0.4}$ distance from fixed point μ_t^* in the attracting F_t-dynamics. In orange, a logarithmic slope of gradient 0.6, indicating a local fractal dimension of around 1.6 for the SRB measure of F_t at the fixed point. The histogram was obtained from a single time series μ_n of which $400,000$ timesteps had $d_{H_{0.4}}(\mu_n, \mu_t^*) \leq 0.003$.

the fixed point and thus the homoclinic tangency. As a consequence, we can conclude that, not just the map F, but the actual *large-scale dynamics on the attractor* are non-uniformly hyperbolic. This is in contradiction of Hypothesis 1.

7 Conclusion

The chaotic hypothesis (Hypothesis 1) makes a broad claim about the large-scale behaviour of complex chaotic systems. This paper provides a counterexample to it in a mean-field coupled system. We studied this system's thermodynamic limit, which encodes the large-scale dynamics and which the chaotic hypothesis therefore predicts to be hyperbolic on its attractor. We have found however that this attractor contains a homoclinic tangency, and the dynamics on it therefore are non-uniformly hyperbolic.

On the other hand, a commonly cited restriction on Hypothesis 1 is that it holds only for *generic* systems: thus, the homoclinic tangency we find could be a special point. However, as a result of having certain genericity properties discussed in Section 6.1, our homoclinic tangency can be expected to generate non-hyperbolic structures on an open set of parameters, following a result of [37]. This results state that for C^∞ diffeomorphisms with one unstable direction but perhaps infinite stable directions, these genericity properties imply the existence of heteroclinic tangencies between stable and unstable manifolds of (non-fixed) hyperbolic points, on an open set of nearby parameters[7] [37]. While our system is not a diffeomorphism, this arises because of very strong stable contracting directions and so fits the spirit of the result. Thus, as well as having a non-uniformly hyperbolic system at one parameter $t = t_{\text{ht}}$, we in fact expect a failure of uniform hyperbolicity on an interval of parameters near $t = t_{\text{ht}}$.

Furthermore, homoclinic tangencies can birth a wide array of exotic objects [9, 32, 53, 37]. Of particular note is the Newhouse phenomenon, where infinitely many sinks may coexist in a single system: because the fixed point of the homoclinic tangency is sectionally dissipative, this peculiar phenomenon occurs on a Baire generic[8] set of parameters t close to t_{ht} [37, 33]. It is a curiosity

[7] Similar results extending finite-dimensional results with more unstable directions [10] may also hold in this infinite-dimensional setting, although they may be difficult to prove.

[8] A Baire generic set is the countable intersection of open dense sets. Baire genericity does not imply a set is of positive measure. For diffeomorphisms of two-dimensional manifolds, the Hausdorff dimension of the set of Newhouse parameters is at least 1/2 [7] and is conjectured to be of measure zero [36].

therefore that for these Newhouse parameters, it is impossible to sample all possible (if unlikely) attracting dynamics. On the other hand, passing from the thermodynamic limit back to finite ensemble size M introduces a small Gaussian noise that will immediately break such dynamical structures.

Although they demonstrate a kind of generic non-uniform hyperbolicity in globally coupled systems, these coupled systems are somewhat atypical of many real-world systems in the sense that they have a uniform all-to-all network structure. In many more realistic systems such as in geophysics, interactions may be spatially localised, and separation between spatial scales may be incomplete. In such systems, emergent noise that forms the first-order correction to the thermodynamic limit may lead to large-scale *stochastic* dynamics [51, 52], which share many helpful similarities with hyperbolic dynamics [55]. Furthermore, even in a globally-coupled systems, physically meaningful coupling types such as attractive or repulsive behaviours may impose their own dynamical constraints which preclude non-uniformly hyperbolic behaviour [25]. Nonetheless, our results show that one cannot guarantee "nice" large-scale dynamics: these depend on the structure of the complex system.

Acknowledgements

This research has been supported by the European Research Council (ERC) under the European Union's Horizon 2020 research and innovation programme (grant agreement No 787304).

The author would like to express her thanks to Georg Gottwald for many helpful discussions. Thank you also to Giovanni Gallavotti for his perspective on the chaotic hypothesis and to Roberto Castorrini for comments on the manuscript.

Appendix

X^α and derivative operators

The perturbation function of f_α as defined in (11) is given explicitly by

$$X_\alpha(q) = g'(\alpha)(1-\mathfrak{d}(f^{-1}(q))^2) = g'(\alpha)\left(1-\left(\frac{2(q-g(\alpha))}{1+\sqrt{1-4g(\alpha)(q-g(\alpha))}}\right)^2\right)$$

Let $X^{(1)}_\alpha := \frac{\partial X_\alpha}{\partial \alpha}$ be its derivative with respect to α.

If we define the operator $\Gamma_t(\mu) := \mathcal{L}_{t\varphi\mu}$ then we have $F_t(\mu) = \Gamma_t(\mu)\mu$. It is standard [1] that the operator

$$D_\mu \Gamma_t v = (\varphi v)\partial_q X_{t\varphi\mu}\Gamma_t(\mu)$$

and by recursion, the Hessian

$$H_\mu\Gamma_t(v,w) = (\varphi v)\partial_q\left(X^{(1)}_{t\varphi\mu}\Gamma_t(\mu) + X_{t\varphi\mu}(D_\mu\Gamma_t v)\right).$$

As a result, the differential and Hessian of F are respectively given by

$$\begin{aligned}(D_\mu F_t)(v) &= \Gamma_t(\mu)v + D_\mu(\Gamma_t v)\mu\\ (H_\mu F_t)(v,w) &= \left(D_\mu\Gamma_t(v+w)\right)\mu + H_\mu\Gamma_t(v,w)\mu.\end{aligned}$$

Further derivatives of the operator $\Gamma_t(\mu)$ (and hence of $F_t(\mu)$) can be obtained from [43].

Proof that the range of $D_\mu F : H_\rho \circlearrowleft$ is dense

We first prove that the range of $\mathcal{L}_\alpha : H_\rho \circlearrowleft$ is dense for any $\alpha \in \mathbb{R}$. Let us first note from (3) that we can decompose $f_\alpha = m_\alpha^{-1} \circ \mathfrak{b}$ where $\mathfrak{b}(x) := x \mod 1$, such that $m_\alpha : E_\rho \mapsto m_\alpha(E_\rho)$ is biholomorphic for some sufficiently small $\rho > 0$. For these $\rho > 0$, transfer operator $\mathcal{L}_\alpha$ can therefore be shown to have the form

$$\mathcal{L}_\alpha h = w_\alpha \ ((I + \mathcal{B})h) \circ m_\alpha$$

for some weight function $w_\alpha : E_\rho \to \mathbb{C}\backslash\{0\}$, where $(\mathcal{B}\chi)(z) := \chi(z-1)$. We would like to show that for any $\psi \in H_\rho$ and $\epsilon > 0$ there exists $h \in H_\rho$ such that $\|\psi - \mathcal{L}_\alpha h\|_{H_\rho} \leq \epsilon$. This is to say that we would like to find an h such that the following is small:

$$\sup_{z \in m_\alpha(E_\rho)} \left| ((I + \mathcal{B})h)(z) - \frac{\psi(m_\alpha^{-1}(z))}{w_\alpha(m_\alpha^{-1}(z))} \right| \tag{16}$$

By the Stone-Weierstrass theorem, there exist a series of polynomials $\{p_n\}_{n\in\mathbb{N}}$ approximating the continuous second term in (16) arbitrarily closely on $m_\alpha(E_\rho)$. If $\mathcal{E}_\delta(z) := e^{\delta z}$, it is also possible to choose $\delta > 0$ such that $\mathcal{E}_\delta - 1$ is arbitrarily small on $m_\alpha(E_\rho)$. Let us therefore choose

$$h = \sum_{i=1}^{\infty} (-\mathcal{B})^i \mathcal{E}_\delta p_n.$$

This function lies in H_ρ because $\mathcal{E}_\delta p_n$ is entire and decays exponentially as $\Re z \to -\infty$, uniformly for bounded $\Im z$. Furthermore, $(I + \mathcal{B})h = \mathcal{E}_\delta p_n$, giving us what is required, that is, the density of the range of $\mathcal{L}_\alpha : H_\rho \circlearrowleft$.

We now show that $D_\mu F_t(H_\rho) \supseteq \mathcal{L}_\alpha(H_\rho)$, which will deliver us the density of the range of $D_\mu F_t$. We have from (10) that

$$D_\mu F_t h = \mathcal{L}_{t\varphi\mu} h - \varphi h \ t\mathcal{L}_{t\varphi\mu} \partial_q X_{t\varphi\mu}.$$

Note now that $u(x) = \frac{\pi}{2} \sin \pi x$ lies in H_ρ with $\varphi u = 1$, and, because it is odd, lies in the kernel of all the $\mathcal{L}_\alpha$. Hence, for any $h \in H_\rho$ we can set $\tilde{h} = h - (\varphi h)u$ so that $\varphi\tilde{h} = 0$ and thus

$$D_\mu F_t \tilde{h} = \mathcal{L}_{t\varphi\mu} \tilde{h} = \mathcal{L}_{t\varphi\mu} h,$$

implying the required inclusion of images.

References

[1] V. Baladi, *Linear response, or else*, in ICM Seoul 2014, Proceedings, Volume III, Aug 2014, pp. 525–545.

[2] V. Baladi, *Dynamical Zeta Functions and Dynamical Determinants for Hyperbolic Maps*, Springer, Berlin, 2016.

[3] V. Baladi, M. Benedicks, and D. Schnellmann, *Whitney–Hölder continuity of the SRB measure for transversal families of smooth unimodal maps*, Inventiones mathematicae, 201 (2015), pp. 773–844.

[4] O. F. Bandtlow and J. Slipantschuk, *Lagrange approximation of transfer operators associated with holomorphic data*, arXiv preprint arXiv:2004.03534, (2020).

[5] T. L. Bell, *Climate sensitivity from fluctuation dissipation: Some simple model tests*, Journal of the Atmospheric Sciences, 37 (1980), pp. 1700–1707.

[6] P. Berger, *Generic family with robustly infinitely many sinks*, Inventiones mathematicae, 205 (2016), pp. 121–172.

[7] P. Berger and J. De Simoi, *On the Hausdorff dimension of Newhouse phenomena*, in Annales Henri Poincaré, vol. 17, Springer, 2016, pp. 227–249.

[8] A. Blumenthal, J. Xue, and L.-S. Young, *Lyapunov exponents for random perturbations of some area-preserving maps including the standard map*, Annals of Mathematics, (2017), pp. 285–310.

[9] C. Bonatti and L. J. Díaz, *Persistent nonhyperbolic transitive diffeomorphisms*, Annals of Mathematics, 143 (1996), pp. 357–396.

[10] C. Bonatti, L. J. Díaz, and E. R. Pujals, *A c1-generic dichotomy for diffeomorphisms: weak forms of hyperbolicity or infinitely many sinks or sources*, Annals of Mathematics, (2003), pp. 355–418.

[11] R. Bowen, *Equilibrium states and the ergodic theory of Anosov diffeomorphisms*, Lecture notes in mathematics, 470, Springer, Berlin, 2nd ed., 2008.

[12] J.-R. Chazottes and B. Fernandez, *Dynamics of coupled map lattices and of related spatially extended systems*, vol. 671, Springer Science & Business Media, 2005.

[13] M. D. Chekroun, J. D. Neelin, D. Kondrashov, J. C. McWilliams, and M. Ghil, *Rough parameter dependence in climate models and the role of Ruelle-Pollicott resonances*, Proceedings of the National Academy of Sciences, 111 (2014), pp. 1684–90.

[14] M. Ciszak, S. Olmi, G. Innocenti, A. Torcini, and F. Marino, *Collective canard explosions of globally-coupled rotators with adaptive coupling*, 2021.

[15] F. Cooper and P. Haynes, *Assessment of the fluctuation-dissipation theorem as an estimator of the tropospheric response to forcing*, Preprint, (2013).

[16] S. Galatolo, *Self consistent transfer operators in a weak coupling regime. Invariant measures, convergence to equilibrium, linear reponse and control of the statistical properties*, arXiv preprint arXiv:2105.12388, (2021).

[17] G. Gallavotti, *Nonequilibrium and fluctuation relation*, Journal of Statistical Physics, 180 (2020), pp. 172–226.

[18] G. Gallavotti and E. G. D. Cohen, *Dynamical ensembles in nonequilibrium statistical mechanics*, Phys. Rev. Lett., 74 (1995), pp. 2694–2697.

[19] ——, *Dynamical ensembles in stationary states*, Journal of Statistical Physics, 80 (1995), pp. 931–970.

[20] S. Gouëzel and C. Liverani, *Banach spaces adapted to anosov systems*, Ergodic Theory and dynamical systems, 26 (2006), pp. 189–217.

[21] A. Gritsun, *Statistical characteristics, circulation regimes and unstable periodic orbits of a barotropic atmospheric model*, Philosophical Transactions of the Royal Society A: Mathematical, Physical and Engineering Sciences, 371 (2013), p. 20120336.

[22] D. Henry, *Geometric theory of semilinear parabolic equations*, vol. 840, Springer, 2006.

[23] K. Kaneko, *Self-consistent Perron-Frobenius operator for spatiotemporal chaos*, Physics Letters A, 139 (1989), pp. 47–52.

[24] G. Keller, *An ergodic theoretic approach to mean field coupled maps*, in Fractal geometry and stochastics II, Springer, 2000, pp. 183–208.

[25] J. Koiller and L.-S. Young, *Coupled map networks*, Nonlinearity, 23 (2010), p. 1121.

[26] S. P. Kuznetsov, *Possible occurrence of hyperbolic attractors*, in Hyperbolic Chaos, Springer, 2012, pp. 35–56.

[27] J. L. Lebowitz and H. Spohn, *A Gallavotti–Cohen-type symmetry in the large deviation functional for stochastic dynamics*, Journal of Statistical Physics, 95 (1999), pp. 333–365.

[28] V. Lembo, V. Lucarini, and F. Ragone, *Beyond forcing scenarios: Predicting climate change through response operators in a coupled general circulation model*, arXiv preprint arXiv:1912.03996, (2019).

[29] S. Lepri, R. Livi, and A. Politi, *Energy transport in anharmonic lattices close to and far from equilibrium*, Physica D: Nonlinear Phenomena, 119 (1998), pp. 140–147.

[30] V. Lucarini, D. Faranda, J. Wouters, and T. Kuna, *Towards a general theory of extremes for observables of chaotic dynamical systems*, Journal of statistical physics, 154 (2014), pp. 723–750.

[31] V. Lucarini and A. Gritsun, *A new mathematical framework for atmospheric blocking events*, Climate Dynamics, 54 (2020), pp. 575–598.

[32] L. Mora and M. Viana, *Abundance of strange attractors*, Acta mathematica, 171 (1993), pp. 1–71.

[33] S. E. Newhouse, *Diffeomorphisms with infinitely many sinks*, Topology, 13 (1974), pp. 9–18.

[34] ——, *The abundance of wild hyperbolic sets and non-smooth stable sets for diffeomorphisms*, Publications Mathématiques de l'IHÉS, 50 (1979), pp. 101–151.

[35] S. Olver, *ApproxFun*, 2019. Available at `https://github.com/JuliaApproximation/ApproxFun.jl` and in the Julia package repository.

[36] J. Palis, *Open questions leading to a global perspective in dynamics*, Nonlinearity, 21 (2008), pp. 1–37.

[37] J. Palis and M. Viana, *High dimension diffeomorphisms displaying infinitely many periodic attractors*, Annals of mathematics, (1994), pp. 207–250.

[38] A. S. Pikovsky and J. Kurths, *Do globally coupled maps really violate the law of large numbers?*, Phys. Rev. Lett., 72 (1994), pp. 1644–1646.

[39] F. Ragone, V. Lucarini, and F. Lunkeit, *A new framework for climate sensitivity and prediction: a modelling perspective*, Climate Dynamics, 46 (2016), pp. 1459–1471.

[40] D. Ruelle, *Differentiation of SRB states*, Communications in Mathematical Physics, 187 (1997), pp. 227–241.

[41] ——, *Linear response theory for diffeomorphisms with tangencies of stable and unstable manifolds—a contribution to the Gallavotti-Cohen chaotic hypothesis*, Nonlinearity, 31 (2018), p. 5683.

[42] E. Sander, *Homoclinic tangles for noninvertible maps*, Nonlinear Analysis: Theory, Methods & Applications, 41 (2000), pp. 259–276.

[43] J. Sedro, *A regularity result for fixed points, with applications to linear response*, Nonlinearity, 31 (2018), p. 1417.

[44] F. M. Sélley, *A self-consistent dynamical system with multiple absolutely continuous invariant measures*, arXiv preprint arXiv:1909.04484, (2019).

[45] F. M. Sélley and M. Tanzi, *Linear response for a family of self-consistent transfer operators*, Communications in Mathematical Physics, 382 (2021), pp. 1601–1624.

[46] A. Tantet, V. Lucarini, F. Lunkeit, and H. A. Dijkstra, *Crisis of the chaotic attractor of a climate model: a transfer operator approach*, Nonlinearity, 31 (2018), p. 2221.

[47] L. N. Trefethen, *Approximation theory and approximation practice*, Siam, Philadelphia, PA, 2013.

[48] C. M. Van Vliet, *Equilibrium And Non-equilibrium Statistical Mechanics*, World Scientific Publishing Company, 2008.

[49] C. L. Wormell, *Poltergeist*, 2017. Available at `https://github.com/wormell/Poltergeist.jl` and in the Julia package repository.

[50] ——, *Spectral Galerkin methods for transfer operators in uniformly expanding dynamics*, Numerische Mathematik, 142 (2019), pp. 421–463.

[51] C. L. Wormell and G. A. Gottwald, *On the validity of linear response theory in high-dimensional deterministic dynamical systems*, Journal of Statistical Physics, 172 (2018), pp. 1479–1498.

[52] C. L. Wormell and G. A. Gottwald, *Linear response for macroscopic observables in high-dimensional systems*, Chaos: An Interdisciplinary Journal of Nonlinear Science, 29 (2019), p. 113127.

[53] J. A. Yorke and K. T. Alligood, *Cascades of period-doubling bifurcations: a prerequisite for horseshoes*, Bulletin (New Series) of the American Mathematical Society, 9 (1983), pp. 319–322.

[54] L.-S. Young, *Ergodic theory of differentiable dynamical systems*, in Real and complex dynamical systems, Springer, 1995, pp. 293–336.

[55] ——, *Comparing chaotic and random dynamical systems*, Journal of Mathematical Physics, 60 (2019), p. 052701.